Crystal structure of 7,8-dihydroneopterin triphosphate epimerase

Tarmo Ploom[1]*, Christoph Hauβmann[2], Peter Hof[1†], Stefan Steinbacher[1], Adelbert Bacher[2], John Richardson[1] and Robert Huber[1]

Background: Dihydroneopterin triphosphate (H_2NTP) is the central substrate in the biosynthesis of folate and tetrahydrobiopterin. Folate serves as a cofactor in amino acid and purine biosynthesis and tetrahydrobiopterin is used as a cofactor in amino acid hydroxylation and nitric oxide synthesis. In bacteria, H_2NTP enters the folate biosynthetic pathway after nonenzymatic dephosphorylation; in vertebrates, H_2NTP is used to synthesize tetrahydrobiopterin. The dihydroneopterin triphosphate epimerase of *Escherichia coli* catalyzes the inversion of carbon 2′ of H_2NTP.

Results: The crystal structure of the homo-octameric protein has been solved by a combination of multiple isomorphous replacement, Patterson search techniques and cyclic averaging and has been refined to a crystallographic R factor of 18.8% at 2.9 Å resolution. The enzyme is a torus-shaped, D_4 symmetric homo-octamer with approximate dimensions of 65 × 65 Å. Four epimerase monomers form an unusual 16-stranded antiparallel β barrel by tight association between the N- and C-terminal β strands of two adjacent subunits. Two tetramers associate in a head-to-head fashion to form the active enzyme complex.

Conclusions: The folding topology, quaternary structure and amino acid sequence of epimerase is similar to that of the dihydroneopterin aldolase involved in the biosynthesis of the vitamin folic acid. The monomer fold of epimerase is also topologically similar to that of GTP cyclohydrolase I (GTP CH-1), 6-pyrovoyl tetrahydropterin synthase (PTPS) and uroate oxidase (UO). Despite a lack of significant sequence homology these proteins share a common subunit fold and oligomerize to form central β barrel structures employing different cyclic symmetry elements, D_4, D_5, D_3 and D_2, respectively. Moreover, these enzymes have a topologically equivalent acceptor site for the 2-amino-4-oxo pyrimidine (2-oxo-4-oxo pyrimidine in uroate oxidase) moiety of their respective substrates.

Addresses: [1]Max-Planck-Institut für Biochemie, Abteilung Strukturforschung, Am Klopferspitz 18a, D-82152 Martinsried, Germany and [2]Lehrstuhl für Organische Chemie und Biochemie, Technische Universität München, Lichtenbergstrasse 4, D-85747 Garching, Germany.

[†]Present address: Proteros Biostructures GmbH, Am Klopferspitz 19, D-82152 Martinsried, Germany.

*Corresponding author.
E-mail: ploom@biochem.mpg.de

Key words: crystal structure, 7,8-dihydroneopterin aldolase, 7,8-dihydroneopterin triphosphate epimerase, guanosine triphosphate cyclohydrolase I, 6-pyruvoyl tetrahydropterin synthase, uroate oxidase

Received: 6 January 1999
Revisions requested: 27 January 1999
Revisions received: 19 February 1999
Accepted: 22 February 1999

Published: 28 April 1999

Structure May 1999, 7:509–516
http://biomednet.com/elecref/0969212600700509

Introduction

Dihydroneopterin triphosphate (H_2NTP) is the first committed intermediate in the biosynthetic pathways of folate (in plants and microorganisms) and of tetrahydrobiopterin (in insects and vertebrates). An enzyme that catalyzes the epimerization of the 2′ carbon (Figure 1) of H_2NTP has been found in *Escherichia coli*. The biological role of this enzyme and its reaction product, dihydromonapterin triphosphate (H_2MTP), however, remains to be clarified.

E. coli mutants with a deletion of the *folX* gene, which specifies the epimerase, grow normally in minimal medium. Recently the *folX* gene has been cloned, sequenced and overexpressed [1]. Recombinant epimerase forms a homo-octamer as shown by sedimentation equilibrium analysis. The presence of magnesium ions is required for activity. The protein shows 22% sequence identity to dihydroneopterin aldolase from *Haemophilus influenzae*. In line with the sequence similarity between epimerase and aldolase recent studies showed that epimerase can catalyze the aldol-type cleavage of dihydroneopterin, albeit at a lower rate than pteridine aldolase [2].

In *Comamonas* sp., the tetrahydro form of L-monapterin has been reported to serve as a coenzyme in the enzymatic hydroxylation of aromatic amino acids [3]. It has also been suggested that the cyclic monophosphate of L-monapterin acts as a cofactor for alcohol dehydrogenase in *Methylococcus capsulatus* [4]. It was observed that *Dictyostelium discoideum* is chemotactically attracted by L-monapterin during the developmental phase after starvation. The implication is that monapterin is involved in cell sorting [5].

E. coli cells excrete L-monapterin during their logarithmic growth phase. At the switch from the logarithmic to the stationary phase there is a burst-increase in excretion

Figure 1

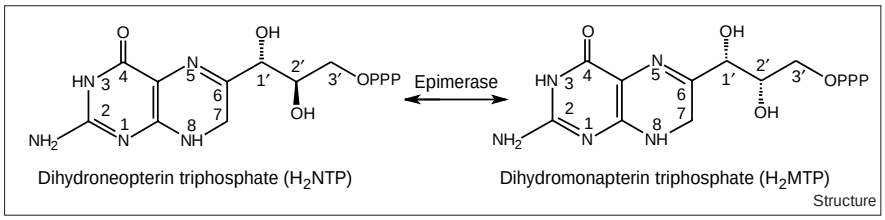

The reaction catalyzed by epimerase. Dihydroneopterin triphosphate is converted to the mixture of dihydroneopterin triphosphate and dihydromonapterin triphosphate.

of L-monapterin so it might be a useful marker for cell proliferation [6].

This paper reports the crystal structure of epimerase from *E. coli*. The structure shows surprising similarity with the structures of 6-pyruvoyl tetrahydropterin synthase [7], GTP cyclohydrolase I [8], 7,8-dihydroneopterin aldolase from *E. coli* (TP, unpublished results) and with both domains of uroate oxidase [9].

Results and discussion

Secondary and tertiary structure

The crystal structure of *E. coli* epimerase was solved by isomorphous replacement, Patterson search calculations between different crystal forms and cyclic averaging. The crystallographic model comprises residues 2–120, which fold into a compact, single-domain α plus β structure (Figure 2).

The sequential four-stranded antiparallel β sheet is composed of residues 5–17, 30–41, 93–103 and 109–119. Layered on one side of this β sheet, a short α helix (residues 42–46) and two long antiparallel α helices (residues 57–69 and 76–87) are inserted in a sequence segment between β strands 2 and 3. Between strands 1 and 2, there is a 13-residue insert containing a short α helix (residues 23–27) that is situated on the same face of the β sheet as the other helices. The monomer has an ellipsoidal shape with dimensions $60 \times 20 \times 20$ Å and is topologically similar to tetrahydrobiopterin biosynthetic enzymes as it also has a ββααββ fold. The hydrophobic core of the epimerase monomer is formed by nonpolar residues of the β sheets and the α helices.

Tetramer and octamer assembly

Epimerase in solution is shown to be an octamer by sedimentation equilibrium analysis [2]. The crystal structure of epimerase shows that the monomers related by fourfold symmetry assemble by tight hydrogen bonding between the N-terminal and C-terminal β strands of adjacent monomers (Figure 3). A 16-stranded antiparallel β barrel is thus formed, surrounded by a ring of α helices. The tetramer is torus-shaped with 65 Å diameter and a height of 30 Å and encloses a hydrophilic pore of 20 Å diameter. The monomers are held together by a perfect hydrogen-bonding network between antiparallel β strands of residues 7–14 of the N-terminal strand and residues 108–115 of the C-terminal strand. The tetramer assembly is additionally stabilized by salt bridges (Glu49–Lys78, Arg9–Glu99 and Lys11–Asp101) and several hydrophobic contacts (Ala6–Leu116, Ile10–Val112 and Leu13–Ala109). The accessible surface of the tetramer is decreased by 26% when compared with isolated monomers.

A local twofold axis perpendicular to the local fourfold axis relates two tetramers that arrange in a head-to-head fashion to form the octamer (Figure 4). The contact region between tetramers is formed by symmetrical contacts

Figure 2

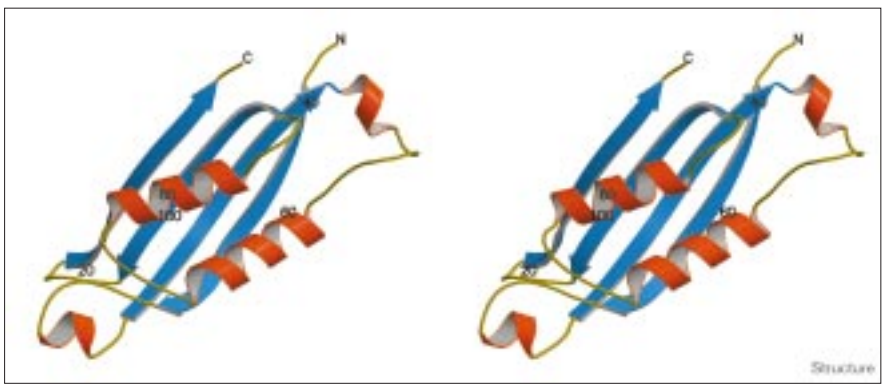

Fold of the monomer of epimerase. The β strands and α helical regions are shown in blue and red, respectively. The connecting loops, which lack extended secondary structure elements, are shown in yellow.

Figure 3

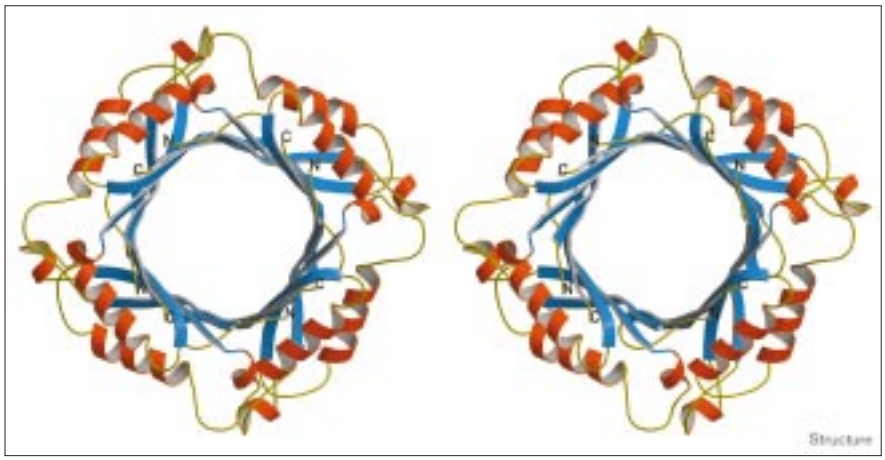

The epimerase tetramer viewed along the fourfold symmetry axis. The four-stranded β sheets of all subunits assemble to a 16-stranded antiparallel β barrel, which is surrounded by a layer of helices. The tetramer is cylindrically shaped with an inner diameter of 20 Å and an outer diameter of 65 Å. The β strands and α helical regions are shown in blue and red, respectively. The connecting loops, which lack extended secondary structure elements, are shown in yellow.

between the regions 22–30 and 14–16, and 104–109 and 14–16, respectively. The surface per monomer covered in the tetramer–tetramer contact is only 6% of the monomer surface, suggesting a much tighter interaction in the tetramer compared with that in the octamer.

Comparison with structurally similar enzymes

The structure of the epimerase is topologically similar to that of 7,8-dihydroneopterin aldolase (DHNA) (TP, unpublished results) [10], 6-pyruvoyl tetrahydropterin synthase (PTPS) [7], the C-terminal domain of GTP cyclohydrolase-I (GTP CH-1), residues 91–221 [8], and domains 1 and 2 of uroate oxidase (UO1 and UO2) [9] (Figure 5). GTP CH-I, PTPS and DHNA are involved in the biosynthesis of pterin compounds. More specifically, aldolase catalyzes the conversion of 7,8-dihydroneopterin or 7,8-dihydromonapterin to 6-hydroxy-7,8-dihydropterin, GTP CH-I catalyzes the conversion of guanosine triphosphate to H_2NTP, and PTPS converts H_2NTP to 6-pyruvoyl tetrahydrobiopterin. The substrates of epimerase, DHNA and PTPS as well as the product of GTP CH-I are pterin-based. This might indicate the existence of a specific 'pterin' fold to recognize and catalyze conversions of substrates based on the 2-amino-4-oxo-pyrimidine ring. The 'pterin' fold is also used to recognize the 2-oxo-4-oxo-pyrimidine ring in UO, which catalyzes the conversion of uric acid to allotonin. The topological alignment (Figure 6) of epimerase with PTPS, GTP CH-I, UO1 and UO2 shows only about 10% sequence identity, whereas the identity to DHNA is 22%. The enzymes do not share conserved residues except a glutamate (glutamine in UO2) that is involved in pterine recognition (Glu77 in epimerase). They do, however, share a specific distribution of hydrophobic residues in the β strands and in the α helices that are involved in the formation of the hydrophobic core of the pterin fold. Superposition of topologically equivalent amino acids in the four β strands and the two major α helices results in a root mean squared deviation (rmsd) fit between 71 Cα positions of 1.60 Å for GTP CH-I, 2.10 Å for PTPS, 1.57 Å for UO1, 1.86 Å for UO2 and 1.05 Å for *E. coli* DHNA (TP, unpublished results) compared with epimerase. Although the characteristic main secondary structure elements of the pterin fold are conserved within the five enzymes, several insertions and deletions involving not only loops but also short

Figure 4

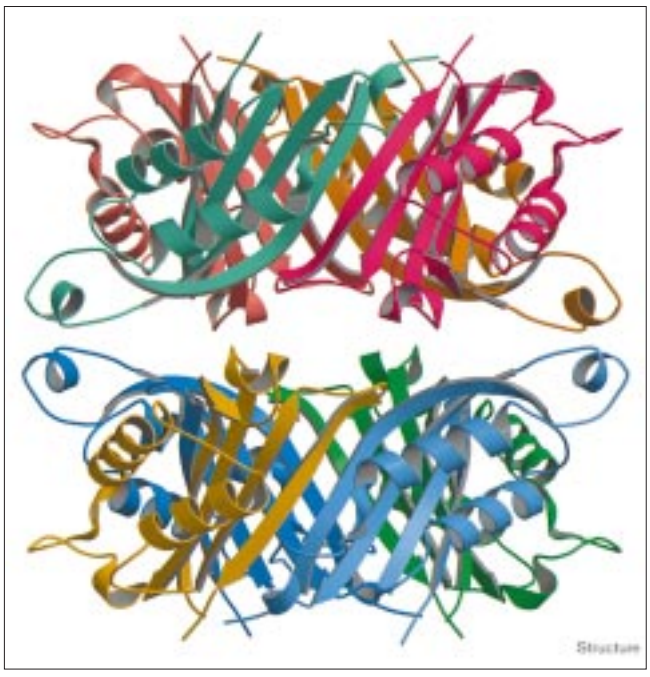

Ribbon presentation of the epimerase octamer viewed along the twofold axis. Two tetramers arrange in head-to-head fashion to form an enzymatically active octamer. Each colour represents a different subunit.

Figure 5

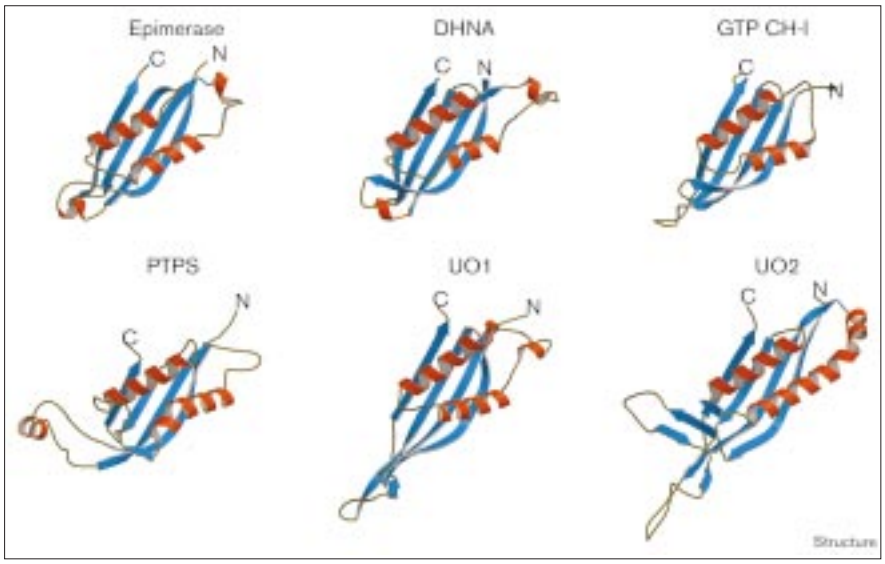

Structural gallery of the monomers of 'pterin' fold enzymes: epimerase, DHNA, the C-terminal domain of GTP CH-I (residues 91–206), PTPS, uroate oxidase domains 1 (residues 1–137) and 2 (residues 138–295). The β strands and α helical regions are shown in blue and red, respectively. The connecting loops, which lack extended secondary structure elements, are shown in yellow.

secondary structure elements occur in the regions outside the four β strands and the two α helices.

The structural similarity of these proteins extends beyond the level of tertiary structure. Even though the formation of the β barrels of the quaternary structure involves a different number of subunits and different orders of rotational symmetry, they share a common architecture. In PTPS, which exhibits threefold symmetry, hydrogen bonding between β strands of neighboring monomers leads to a 12-stranded antiparallel β barrel surrounded by a ring of six α helices. Epimerase and DHNA show fourfold symmetry and, by the same mode of hydrogen bonding, a 16-stranded β barrel with eight α helices is formed. In UO the hydrogen bonding between two structurally identical monomers also leads to the formation a of 16-stranded

Figure 6

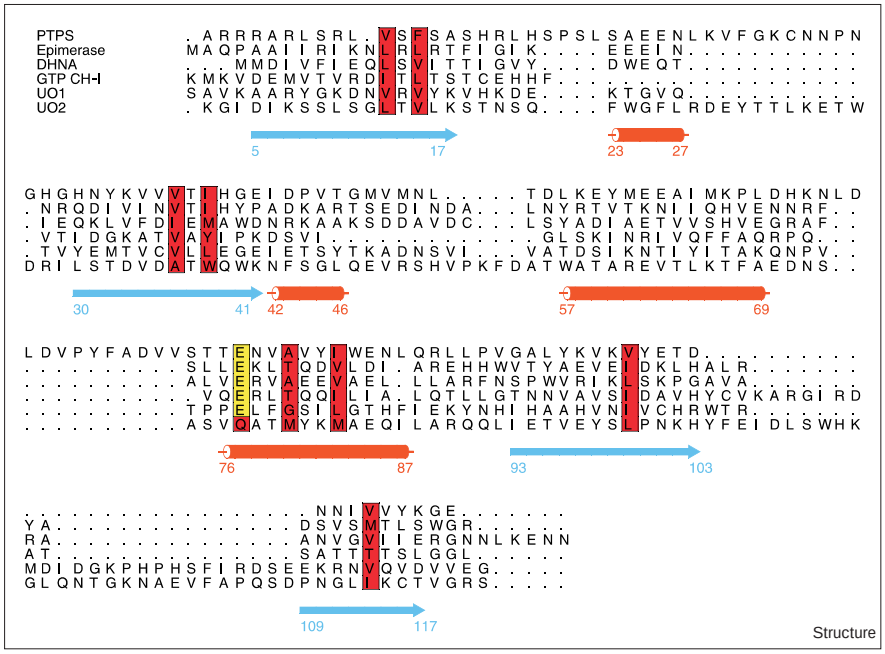

Topological alignment of the 'pterin' fold enzymes. The conserved residues are boxed in yellow and similar residues in red. The only conserved residue is Glu77 of epimerase. Equivalent residues in GTP CH-I, PTPS and DHNA are anchors for the 2-amino-4-oxo pyrimidine moiety of the substrate. β Strands of epimerase are depicted by blue arrows, α helices by orange rods.

Figure 7

Stereoview of the putative active site of epimerase. A pterin-binding pocket is formed by residues from two adjacent monomers. At the bottom of the pocket Glu77 and the mainchain amide of Leu75 could serve as acceptor for the pterin moiety. Two bases, Lys102 and Arg58, could facilitate proton abstraction on both stereoisomers, H_2NTP and H_2MTP. Carbon atoms are shown in green, oxygen in red and nitrogen in blue.

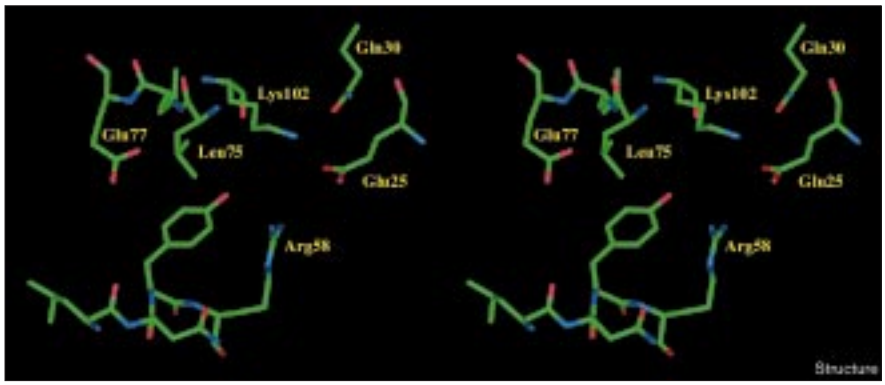

β barrel with eight α helices. GTP CH-I with its fivefold symmetry forms a 20-stranded β barrel with ten α helices. Closed structures with dihedral symmetry are generated in all cases by diad axes perpendicular to the main symmetry axis, D_3 in PTPS, D_4 in epimerase and DHNA, D_5 in GTP CH-I and D_2 in UO1 and UO2.

All of these structures enclose a solvent-filled pore. The hexamer of PTPS encloses a strongly positively charged cavity of dimensions $20 \times 20 \times 15$ Å, as does the decamer of GTP CH-I, with dimensions of $30 \times 30 \times 15$ Å. The cavities in PTPS and GTP CH-I are accessible through the pores in the center of the barrels. The homotetrameric UO encloses a pore that is 50 Å in length and 12 Å in diameter, the DHNA encloses a pore with a diameter of at least 13 Å and epimerase encloses a pore with a diameter of 15 Å. The tunnel wall in DHNA is strongly negatively charged, whereas the tunnel wall in epimerase and UO is heterogeneously charged. It has been proposed for PTPS that the pore could act as a channel for the substrate, H_2NTP, which is highly negatively charged by its triphosphate moiety and might enter the arginine-coated pore by attractive electrostatic forces of the basic residues [7]. In epimerase, which uses the same substrate as PTPS, however, charges are balanced inside the pore. The role of the pore in these structures therefore remains elusive.

The different oligomeric state of the pterin enzymes results in different tilts of the β strands with respect to the main rotation axes and to the perpendicular twofold axis and in different sizes of central cavities. These different geometrical features are accompanied by small changes in secondary structure elements and loops. The basic fold of four β strands and two antiparallel α helices remains unaltered. Although the enzymes with the pterin fold share common features of their substrates and products, the reactions catalyzed are very diverse. In all cases they are intramolecular reactions, however, without an overall oxidation-state change. These observations suggest the existence of a superfamily of enzymes that catalyze the remodeling of substrates based on the 2-amino-4-oxo or 2-oxo-4-oxo pyrimidine ring system.

The structure of the active site

The topological similarity of epimerase to PTPS, GTP CH-I and DHNA, for which structural information of substrate binding is available, suggests the location of the active site. The only conserved residue in the topological alignment of these four structures is Glu77, which serves as an anchor for the 2-amino-4-oxo pyrimidine ring in all three enzymes. The putative pterin-binding pocket in epimerase is located at the interface of two adjacent monomers and is formed by Leu75, Tyr57 and the backbone of Leu55 and Leu76 (Figure 7). The pterin could be anchored to Glu77 and its binding could be enhanced by hydrogen bonds to the backbone and by interactions with surrounding hydrophobic residues. The anchoring of a pterin would direct the sidechain 2′ hydroxyl group into close proximity with Arg58, Lys102, Glu25 and Gln30. A cluster of basic residues (Lys22 and Arg107) near the entrance of the active site might serve to bind the triphosphate moiety of substrate and product. The active site of epimerase is very similar to that of DHNA; six out of seven residues are highly conserved between them. For a precise definition of substrate binding, the structures of epimerase in complex with substrate or product will have to be determined.

The catalytic mechanism

A possible catalytic mechanism of epimerase (Figure 8) might start with protonation of N5 of the pterin ring, followed by an imin–enamine tautomerization step, which would increase the acidity of the C2′ hydroxyl group proton. The bases Arg58 and Lys102 might be involved as proton abstractors from the C2′ hydroxyl group, initiating rearrangements leading to the cleavage of the C1′–C2′ carbon bond [2]. These two bases are located symmetrically at the different faces of the substrate sidechain facilitating proton abstraction from the hydroxyl group of both stereoisomers, H_2NTP and

Figure 8

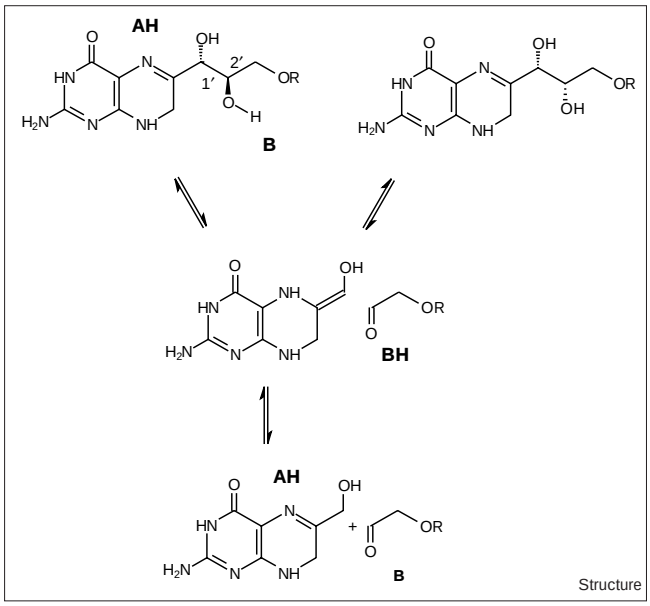

Hypothetical reaction mechanism for aldolase-one and epimerase-type reactions [2]. For details see the Discussion section. AH represents a general acid and B represents a general base. The figure shows the interconversion of phosphorylated dihydroneopterin, dihydromonapterin and 6-hydroxymethyl-dihydropterin.

H_2MTP. It is known that epimerase also catalyzes cleavage reactions of 7,8-dihydroneopterin and 7,8-dihydromonapterin [2] to form 6-hydroxy-7,8-dihydropterin and glycolaldehyde. Epimerization might occur if the reaction products resulting from cleavage, instead of being released from the enzyme, react in the reverse direction without stereocontrol, as happens in phosphorylated substrates such as H_2NTP and H_2MTP. The catalytic mechanisms of epimerase and DHNA are very similar [2]. In the reaction of epimerase or DHNA with 7,8-dihydroneopterin or 7,8-dihydromonapterin the glycolaldehyde is released from the enzyme resulting in a cleavage reaction. In the reaction of epimerase with H_2NTP the triphosphate moiety is well bound to the enzyme and reacts in the reverse direction without stereocontrol, resulting in the epimerization reaction.

Biological implications

Dihydroneopterin triphosphate (H_2NTP) is the central substrate in the biosynthesis of tetrahydrofolic acid and tetrahydrobiopterin. The former serves as an enzyme cofactor in amino acid and purine biosynthesis, the latter is used as a cofactor in amino acid hydroxylation and in nitric oxide synthesis. In bacteria, H_2NTP enters the folic acid biosynthesis pathway after nonenzymatic dephosphorylation. In vertebrates, which cannot synthesize folic acid, H_2NTP is used to synthesize tetrahydrobiopterin in two consecutive steps. Epimerase catalyzes the conversion of this important compound to dihydromonapterin triphosphate (H_2MTP).

We present the crystal structure of epimerase from *E. coli*. The enzyme forms a homo-octamer with overall dimensions of $65 \times 65 \times 65$ Å. Epimerase shows a fold that is conserved between other enzymes involved in the biosynthesis of pterin compounds, such as GTP cyclohydrolase I (GTP CH-I), 6-pyruvoyl tetrahydropterin synthase (PTPS) and 7,8-dihydroneopterin aldolase (DHNA). The oligomerization model to form antiparallel β barrels is related in this family even though it led to D_2, D_3, D_4 and D_5 symmetry. The enzymes share similar pterin folds consisting of four β strands and two α helices. In a topological alignment of these structures only a glutamate (glutamine in uroate oxidase domain 2, UO2) is conserved that serves as an anchor for pterin binding.

Materials and methods

Crystallisation and data collection

The epimerase of *E. coli* was purified from a recombinant strain as previously described [1]. The enzyme was concentrated using Ultrafree concentration units (Millipore products) with a molecular mass cut-off of 30 kDa and was dialyzed against 5 mM Tris-HCl, pH 7.8, containing 25 mM NaCl. Crystals were grown at 20°C by vapor diffusion. For the preparation of sitting drops, enzyme solution and precipitant solution were mixed at a ratio of 1:2. Incomplete sparse matrices were used to search for initial crystallization conditions and further optimization led to four different crystal forms. Form A was grown from 1.3 M K/Na-Tartrate, 0.1 M Tris-HCl, pH 8.8, and diffracted to at least 2.0 Å. Form A crystallizes in the space group P2(1)2(1)2(1) with cell dimensions a = 91.3 Å, b = 91.3 Å, c = 146.1 Å, $\alpha = \beta = \gamma = 90°$. Although crystal form A showed anisotropic mosaicity it was used to obtain initial phases by multiple isomorphous replacement. Form B, diffracting to 2.8 Å and grown under the same conditions as form A with 0.1 M 1,2,3-heptanetriol added, crystallizes in the space group C222(1), with cell dimensions a = 84.7 Å, b = 130.9 Å, c = 251.6 Å, $\alpha = \beta = \gamma = 90°$. Form C, diffracting to 2.9 Å and grown from 35% ethylene glycol, crystallizes in the space group P4(1) with cell dimensions a = 69.9 Å, b = 69.9 Å, c = 237.2 Å, $\alpha = \beta = \gamma = 90°$. The asymmetric unit of all crystal forms contained eight monomers. Form C was used for the final structure refinement. Form D was grown from 24% jeffamine M-600, 0.1 M MES, pH 6.6, diffracted to 2.4 Å and belonged to the space group I422. Unfortunately, the cumulative distribution of intensities of form D showed strong twinning.

Data were collected on a MAR Research imaging plate detector with graphite-monocromatized Cu-Ka-α radiation from a Rigaku RU200 rotating-anode generator, operating at 50 kV and 100 mA and equipped with a Rigaku mirror system. Intensities of reflections were integrated with MOSFLM [11], data were scaled in ROTAVATA [12], merged with AGROVATA [12] and intensities were converted to structure-factor amplitudes using TRUNCATE [12].

Structure determination

The structure of epimerase was solved by a combination of multiple isomorphous replacement, Patterson search calculations, optimization of the local symmetry operators by cyclic averaging and final cyclic averaging.

Heavy-atom derivatives were made by soaking crystals of form A in harvesting buffer (1.4 M K/Na-Tartrate, 0.1 M Tris-HCl, pH 8.8) with heavy-metal compounds (1 mM) for 24 h. The native Patterson map of crystal form A shows two strong pseudo-centering peaks and one weak

pseudo-origin peak indicating noncrystallographic translational symmetry. Local symmetry was used in the interpretation of the isomorphous difference Patterson maps. The observed heavy-atom sites were confirmed by cross-difference Fourier syntheses. The search in Patterson and Fourier space was performed with the PROTEIN program package [13]. Three heavy-atom derivatives and 27 sites were used for the final phase calculation in the program SHARP [14], which gave an overall figure of merit of 0.4 (20–2.7). The correct hand of a consistent set of heavy-atom sites was determined by using anomalous dispersion data using the program MLPHARE [15]. Solvent flattening, histogram matching and skeletonization in DM [12] were used for further improvement of the phases (cumulative figure of merit 0.61).

An electron-density map calculated at 2.7 Å showed clearly the molecular boundary and several secondary structure elements. In order to improve the phases the noncrystallographic symmetry operators were refined using density correlation of the electron density within an octamer. For that purpose the electron density of the octamer was shifted/translated using the proposed operators and the correlation to the starting electron density was computed. The density correlation searches were carried out with the program package MAIN [16]. Self-rotation calculations of the data of form A indicated that the local fourfold axis was exactly parallel to the crystallographic c-axis. The center of the fourfold axis was exactly at x = 1/4, y = 1/4. The self-rotation function had shown that the local twofold axes are perpendicular to the local fourfold axis, confirming that the octamer in the asymmetric unit has 422 symmetry. In order to find the exact molecular center and the direction of the twofold axes, additional density correlation searches were performed. Surprisingly, two different centers (4.0 Å apart) and orientations (22.5° apart) for the local twofold axes inside the electron density were found, indicating disorder. Trials to improve the electron density by twofold cyclic averaging resulted in a diffuse electron density and gave a back-transformation R factor of 30%. Several trials of model building were made, but the R_{free} remained high, confirming disorder of crystal form A. The cumulative intensity distribution did not show characteristic curves of twinning.

The electron density of the octamer from crystal form A was used to interpret the data of the crystal forms B and C by Patterson search calculations. The electron density of the octamer was isolated and transformed into an artificial P1 cell using the program MAIN [16] and converted into AMoRe format using the program e2a [17]. Rotation and translation searches were performed using AMoRe [17]. A rotation solution that confirmed self-rotation was found for crystal form B, although no solution for translation was found. In the crystal form C we succeeded in finding both rotation and translation solutions.

Preliminary to cyclic averaging in crystal form C a grid search was performed in order to improve the noncrystallographic symmetry operators. The appropriate molecular center and orientation of the fourfold local axis within the electron density of the octamer was known from the structure solution using form A. Grid searches for the center and orientation of the fourfold axis in crystal form C were performed, with the back-transformation R factor as optimization criteria. The electron density was moved inside the cell to a proposed position and cyclic averaging was performed using the corresponding operators from the electron density of the octamer. The search was carried out with the program MAIN using data between 15 and 5 Å. The translation search revealed a strong single minimum of the back-transformation R factor at x = 68.4, y = 36.4. The Z parameter is not fixed in P4(1). The orientation search slightly improved the orientation found from the AMoRe solution. The orientation of the fourfold local symmetry axis is 77.6°, 87.7° in polar angle ZYK convention.

The electron density of the octamer from crystal form A was transformed to the position found by the grid search, and fourfold cyclic averaging was performed using data between 15 and 3.3 Å. The back-transformation R factor dropped to 17% and the resulting electron density was easily interpretable, indicating that crystal form C is ordered.

Table 1

Data collection, phasing and refinement statistics.

	Form C	Form A	K_2PtCl_6	K_2PtCl_6	$(NH_3)_2Pt(NO_2)_2$
Data collection					
Maximum resolution	2.9	2.5	2.7	2.7	3.05
Completeness (%)	94.6	87.0	89.0	91.8	94.8
Total reflections	68,471	112,637	77,260	76,739	57,870
Unique reflections	23,361	36,909	28,615	29,515	23,148
R_{sym}* (%)	11.9	9.7	8.2	10.2	8.0
Phasing statistics					
R_{iso}† (%)	24.1%	27.1%	33.0%		
R_C‡ (%)		0.85	0.78	0.80	
Phasing power	1.47	1.86	1.39		
No. of sites	10	16	13		
Refinement statistics					
No. of protein atoms	9808				
No. of hydrogens	1936				
Used reflections	23,272				
Rms distances (Å)	0.010				
Rms angles (°)	2.055				
Rms deviation between monomers Cα (Å)	0.18				
Mean B protein (Å^2)	33.9				
Rms of bonded B (Å^2)	4.8				
R factor (work set)	18.8				
R factor (test set)§	25.9				

*$R_{sym} = \Sigma_{hkl}\Sigma_i|I(hkl)_i - \langle I(hkl)\rangle| / \Sigma_{hkl}\Sigma_i \langle I(hkl)_i\rangle$. †$R_{iso} = \Sigma_{hkl}|F_{PH}(hkl) - F_P(hkl)| / \Sigma_{hkl}F_P(hkl)$. ‡$R_c = \Sigma_{hkl}||F_{PH}(hkl)| + -|F_P(hkl)|| - F_{Hcalc}(hkl)| / \Sigma_{hkl}||F_{PH}(hkl)| + -|F_P(hkl)||$. §For 5% of the data.

Model building and refinement

The electron-density map was used to trace the protein backbone. Iterative rounds of model building with the program FRODO [18], refinement with XPLOR [19] and eightfold cyclic averaging resulted in a model of the epimerase octamer, consisting of residues 2–120. During refinement, noncrystallographic symmetry restraints were applied.

After temperature-factor refinement and application of bulk-solvent correction [20] the R factor of 18.8% (R_{free} of 25.8%) was obtained for data between 30 and 2.9 Å (Table 1). Two loop regions (20–22, 52–55) have high temperature factors (greater than 60 $Å^2$). Even with the solved structure we were not able to understand the exact type of disorder in the crystal form A.

The rms deviations between the Cα atoms of monomers within the octamer are 0.18 Å. Estimated errors from Luzzati [21] and SigmaA [22] plots are 0.30 Å and 0.35 Å, respectively. The current model comprises 9808 protein atoms. The rms deviations from ideal stereochemistry are 0.010 Å for bond length and 2.06° for bond angles [23]. The dihedral angles of the polypeptide backbone are all located within allowed regions of the Ramachandran diagram [24].

Figures were prepared with the programs Molscript [25], Raster [26] and Alscript [27]. Electrostatic potentials were calculated with the program GRASP [28], and the surface area was calculated with NACCESS [29].

Accession numbers

The coordinates of epimerase have been deposited in the Brookhaven Protein Data Bank with accession code 1B91.

Acknowledgements

This work was supported by EC grant FMRX-CT98-0204 and by the Fonds der Chemischen Industrie. We thank N Colloc`h for providing us the coordinates of uroate oxidase.

References

1. Hauβmann, C., Rohdich, F., Lottspeich, F., Eberhardt, S., Scheuring, J., Mackamul, S. & Bacher, A. (1997). Dihydroneopterin tiphosphate epimerase of *Escherichia coli*: purification, genetic cloning and expression. *J. Bacteriol.* **179**, 949-951.
2. Hauámann, C., Rohdich, F., Schmidt, E., Bacher, A. & Richter, G. (1998). Biosynthesis of pteridines in *Escherichia coli*. Structural and mechanistic similarity of dihydroneopterin triphosphate epimerase and dihydroneopterin aldolase. *J. Biol. Chem.* **273**, 17418-17424.
3. Guroff, G. & Rhoads, C.A. (1969). Phenylalanine hydroxylation by Pseudomonas species (ATCC 11299a). Nature of the cofactor. *J. Biol. Chem.* **244**, 142-146.
4. Urushibara, T., Forrest, H.S., Hoare, D.S. & Patel, R.N. (1971). Pteridines produced by Methylococcus capsulatus. Isolation and identification of a neopterin 2′:3′-phosphate. *Biochem. J.* **125**, 141-146.
5. Tillinghast, H.S. & Newell, P.C. (1987). Chemotaxis towards pteridines during development of Dictyostelium. *J. Cell. Sci.* **87**, 45-53.
6. Wachter, H., Hausen, A., Reider, E. & Schweiger, M. (1980). Pteridine excretion from cells as indicator of cell proliferation. *Naturwissenschaften* **67**, 610-611.
7. Nar, H., Huber, R., Heizmann, C.W., Thöny, B. & Bürgisser, D. (1994). Three-dimensional structure of 6-pyruvoyl tetrahydropterin synthase, an enzyme involved in tetrahydrobiopterin biosynthesis. *EMBO J.* **13**, 1255-1262.
8. Nar, H., Huber, R., Meining, W., Schmid, C., Weinkauf, S. & Bacher, A. (1995). Atomic structure of GTP cyclohydrolase I. *Structure* **3**, 459-466.
9. Colloc`h, N., Hajj, M.E., Bachet, B., L`Hermite, G., Schiltz, M., Prange, T., Castro, B. & Mornon, J.-P. (1997). Crystal structure of the protein drug uroate oxidase-inhibitor complex at 2.05 Å resolution. *Nat. Struct. Biol.* **4**. 947-952.
10. Hennig, M., D`Arcy, A., Hampele, I.C., Page, M.G., Oefner, C. & Dale, G.E. (1998). Crystal structure and reaction mechanism of 7,8-dihydroneopterin aldolase from Staphylococcus aureus. *Nat. Struct. Biol.* **5**, 357-362.
11. Leslie, A.G.w. (1994). MOSFLM Version 5.41 MRC Laboratory of Molecular Biology, Cambridge, UK.
12. Collaborative Computational Project, Number 4 (1994). The CCP4 suite: programs for protein crystallography. *Acta Crystallogr. D* **50**, 760-763.
13. Steigemann, W. (1991). From Chemistry to Biology. *Crystallographic Computing* **5**, 115-125, Oxford University Press, Oxford, UK.
14. La Fortelle, E. & Bricogne, G. (1997). Maximum-likelihood heavy-atom parameter refinement for multiple isomorphous replacement and multiwavelength anomalous diffraction methods. (Sweet, R.M. & Carter, C.W., Jr. eds), pp. 472-494, *Methods Enzymol.* **276**, Academic Press, New York, USA.
15. Otwinowski, Z. (1991). Daresbury Study Weekend proceedings.
16. Turk, D. (1992). Development and usage of a macromolecular graphics program. PhD thesis, Technical University Munich, Germany.
17. Navaza, J. (1994). AMoRe: an Automated Package for Molecular Replacement. *Acta Crystallogr. A* **50**, 157-163.
18. Jones, T.A. (1978). A graphics model building and refinement system for macromolecules. *J. Appl. Crystallogr.* **11**, 268-272.
19. Brünger, A.T. (1992). X-PLOR, Version 3.1: a system for crystallography and NMR. Yale University Press, New Haven, CT, USA.
20. Jiang, J.-S. & Brünger, A.T. (1994). Protein hydration observed by X-ray diffraction: solvation properties of penicillopepsin and neuroaminidase crystal structures. *J. Mol. Biol.* **243**, 100-115.
21. Luzzati, V. (1952). Traitement statistique des erreurs dans la determination des structures cristallines. *Acta. Crystallogr.* **5**, 802-810.
22. Read, R.J. (1986). Improved fourier coefficients for maps using phases from partial structures with errors. *Acta Crystallogr. A* **42**, 140-149.
23. Engh, R.A. & Huber, R. (1991). Accurate bond and angle parameters for X-ray protein structure and refinement. *Acta Crystallogr. A* **47**, 392-394.
24. Ramachandran, G.N. & Sasisekharan, V. (1968). Conformation of polypeptides and proteins. *Adv. Protein Chem.* **23**, 283-437.
25. Kraulis, P.J. (1991). MOLSCRIPT: a program to produce both detailed and schematic plots of protein structure. *J. Appl. Crystallogr.* **24**, 946-950.
26. Merritt, E.A. & Murphy, M.E.P. (1994). Raster3D Version 2.0. A program for photorealistic molecular graphics. *Acta. Crystallogr. D* **6**, 869-873.
27. Barton, G.J. (1993) ALSCRIPT: a tool to format multiple sequence alignments. *Protein Eng.* **6**, 37-40.
28. Nicholls, A., Bharadwaj, R. & Honig, B. (1993). Grasp – graphical representation and analysis of surface properties. *Biophys. J.* **64**, A166.
29. Hubbard, S.J., Campbell, S.F. & Thornton, J.M. (1991). Conformational analysis of limited proteolytic sites in serine proteinase protein inhibitors. *J. Mol. Biol.* **220**, 507-530.